University of New Hampshire

SM51A-2421

Van Allen Probe Observations of Chorus Wave Activity, Source and Seed Electrons, and the Radiation Belt Response During CME and CIR Storms

S. Bingham[1], C. G. Mouikis[1], L. M. Kistler[1], K. Paulson[1], A. J. Boyd[2], C. L. Huang[1], C. Farrugia[1], H. E. Spence[1], C. Kletzing[3]

[1]SSC, Eos, Univ. of New Hampshire, Durham, USA, [2]New Mexico Consortium, Los Alamos, New Mexico, USA , [3]Department of Physics and Astronomy, University of Iowa, Iowa City, Iowa, USA.

Van Allen Probes

Introduction

- Whistler mode chorus waves can contribute to the outer radiation belt by accelerating seed electrons (100s of keV) to higher energies.
- The temperature anisotropy of source electrons (10s of keV) provides the free energy for chorus waves.
- Source & seed electron access to the inner magnetosphere increases during storm times and is dependent on convection, sub-storm activity, and conditioning in the plasmasheet.
- Discrepancies in the characteristic solar wind of CMEs and CIRs create differences in the energy spectrum and composition of the plasmasheet, convection, and substorm activity.

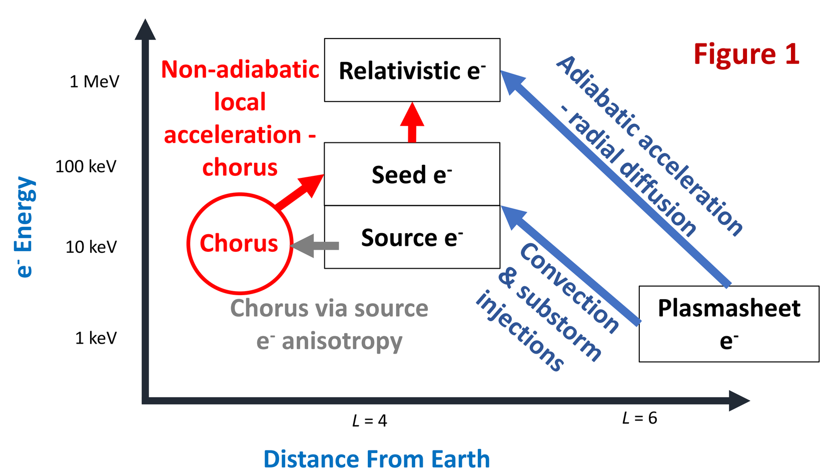

Figure 1

- **Van Allen Probes** (VAPs) are used to construct a **storm phased epoch analysis** of **chorus wave power** and **plasma conditions driving chorus activity** - via a linear theory proxy - **during CME and CIR storms**.
- **Developed w/ VAPs a superposed epoch analysis** of the growth of the **seed** and **radiation belt** electrons vs L^* **during CME/CIR storms**.

VAPs Observations of CME/CIR Chorus Wave Activity

- Gary et al. [2005] developed a **linear theory proxy**, based on plasma measurements, to **infer Chorus wave growth**.
- The **proxy for chorus growth, Σ_e,** is a **product of** the **hot** (1-60 keV) **electron anisotropy** and **hot electron parallel plasma beta**:

$$\Sigma_e = \left(\frac{T_{e,\perp}}{T_{e,\parallel}} - 1\right)\beta^{\alpha}_{e\parallel} \qquad \beta^{\alpha}_{e,\parallel} = \frac{n_e k T_{e,\parallel}}{B^2/2\mu_0}$$

- VAPs used to measure average CME/CIR chorus power and proxy components.
- Figure 4: average VAPs observational values for: (a) observed chorus wave power, (b) hot e- pressure, (c) hot e- plasma beta, (d) hot electron anisotropy: $A = \frac{T_{e\perp}}{T_{e\parallel}} - 1$, and (e) proxy chorus growth.

Chorus power is comparable between CME/CIR storms.

- **Chorus strongest** in **main phase** on **dawn/pre-dawn** sector. In **recovery, wave power decreases**, but remains elevated and **spreads across dayside**.
- **Location of growth proxy, Σ_e, correlates well with measured chorus** power.
- **Chorus power most closely follows source electron plasma beta**.
- **Anisotropy drops during main phase** – waves reduce A_e or fresh e- isotropic.
- **Comparable CME/CIR chorus** activity **agrees with *Spasojevic* [2014]**.

Chorus activity follows drift path of source electrons

- **Source electrons quickly reach dawn w/ enhanced convection** of main phase.
- **In recovery periods, source electrons** have time to **drift across the dayside**, however their overall **flux levels drop as** some drift out through the dayside as **open/closed drift boundaries change**.

Figure 4

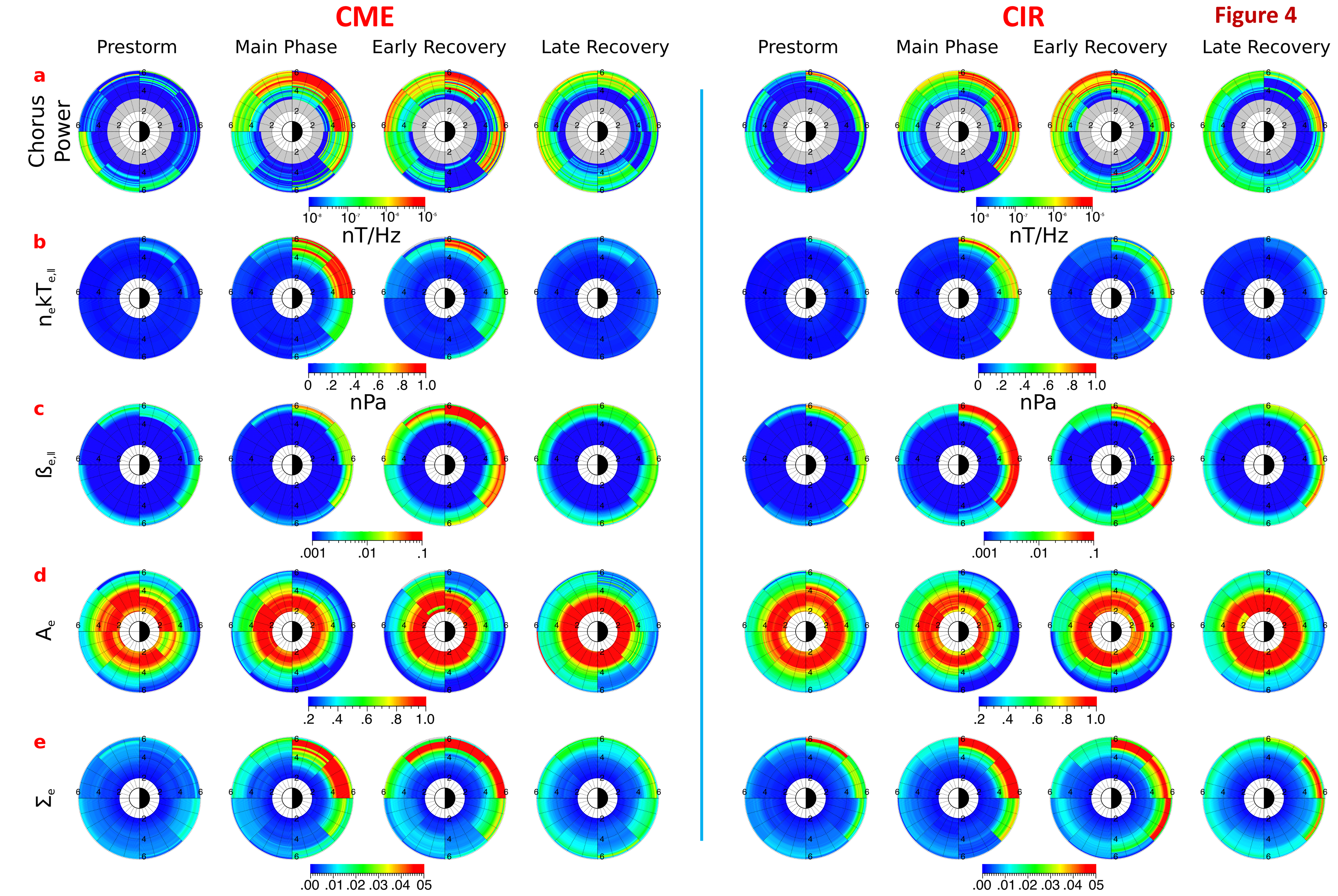

Summary

Storm phase epoch analysis of chorus wave power & linear theory proxy for CMEs/CIRs show:

- **Similar levels of chorus activity during CMEs/CIRs.**
- **Wave power peaks** during **main phase** on **dawn side**, before spreading **across** the **dayside** w/ less intensity **during recovery.**
- **Wave power correlates** well **spatially** w/ **proxy growth**, and **closely follows** the **source electron parallel plasma beta and e- drifts**.

Superposed epoch analysis for fixed seed and RB energies/μ during CME/CIR storms show:

- **Stronger, earlier, and deeper** penetrating **seed e- enhancements during CME storms.**
- **Larger seed enhancement** is possibly driven by **greater substorm activity** and **convection in CME storms.**
- **Greater likelihood** of **overlap** between **seed enhancement** and **chorus during CME storms**.
- **Radiation belt enhancement** occurs **more often during CME** storms and reaches **lower L^*.**
- **PSD profile of CME enhancement** shows some **evidence of local acceleration.**

Data and Storm Selection

Van Allen Probes

- **HOPE** – e- < 60 keV. **MagEIS** – e- 30 keV – 3 MeV.
- **REPT**– e- 1 MeV – 20 MeV. **EMFISIS** – magnetometer and waves instrument.

Storm Selection

- **25 CME** and **35 SIR/CIR Storms** are **identified between 2013-01-01 and 2016-04-16** with a minimum *Dst** between -50 and -150 nT.
- Storm selection **required a single identifiable driver** (CME/CIR). Periods after the start of a second dip in *Dst* were not used.
- Figure 2: **median**, **mean**, and **quartile** superposed epoch solar wind conditions for CMEs/CIRs selected. Main phase normalized to 12 hrs.
- Figure 3: location in *MLT* and *L* of the VAP SC during one orbit for selected CME/CIR storms.

Figure 2

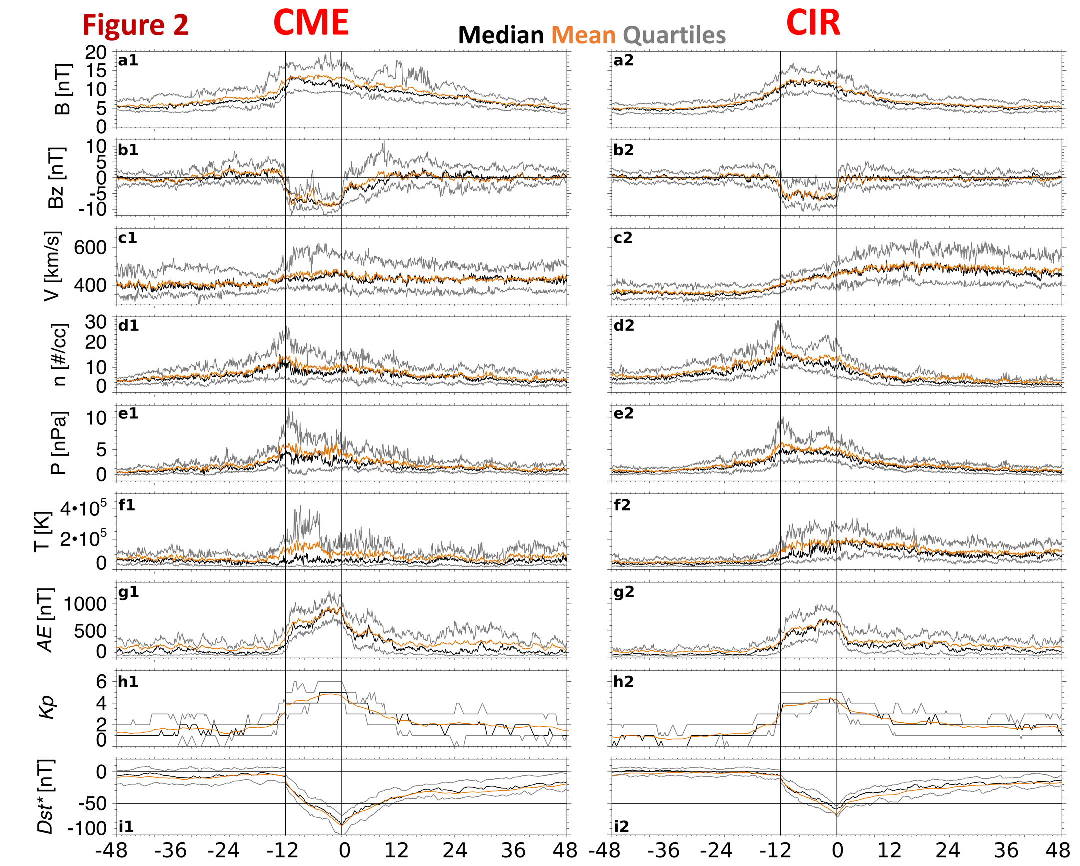

- **CMEs** displayed a **lower *n*, v_{sw}, and T_{sw}** than CIRs.
- **CMEs** had **more substorm activity** and **stronger convection**.

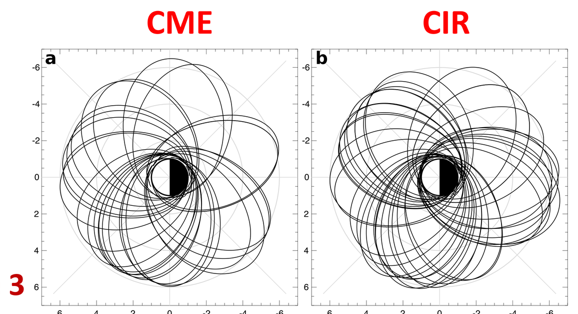

Figure 3

Acknowledgements and References

This work is supported by the NASA NNX14AC88G grant

Boyd, A. J., H. E. Spence, C.-L. Huang, G. D. Reeves, D. N. Baker, D. L. Turner, S. G. Claudepierre, J. F. Fennell, J. B. Blake, and Y. Y. Shprits (2016), Statistical properties of the radiation belt seed population, J. Geophys. Res. Space Physics, 121, 7636–7646, doi:10.1002/2016JA022652.

Gary, S. P., B. Lavraud, M. F. Thomsen, B. Lefebvre, and S. J. Schwartz (2005), Electron anisotropy constraint in the magnetosheath: Cluster observations, Geophys. Res. Lett., 32, L13109, doi:10.1029/2005GL023234.

Spasojevic, M. (2014), Statistical analysis of ground-based cho- rus observations during geo- magnetic storms, J. Geophys. Res. Space Physics, 119, 8299–8317, doi:10.1002/2014JA019975.

Superposed Epoch Analysis of CME/CIR Seed and Radiation Belt Electrons

Flux Response

- Using VAPs we can observe average seed and radiation belt (RB) electron response to CMEs/CIRs at different *L*.
- Figure 5: average flux and chorus power for fixed energies vs L^*.
- Figure 6: average flux in three different L^* ranges.
- Figure 7: change in flux from prestorm vs L^*.
- Epoch *t* = 0 at min *Dst**, main phase times are normalized to 12 hours.

Figure 5

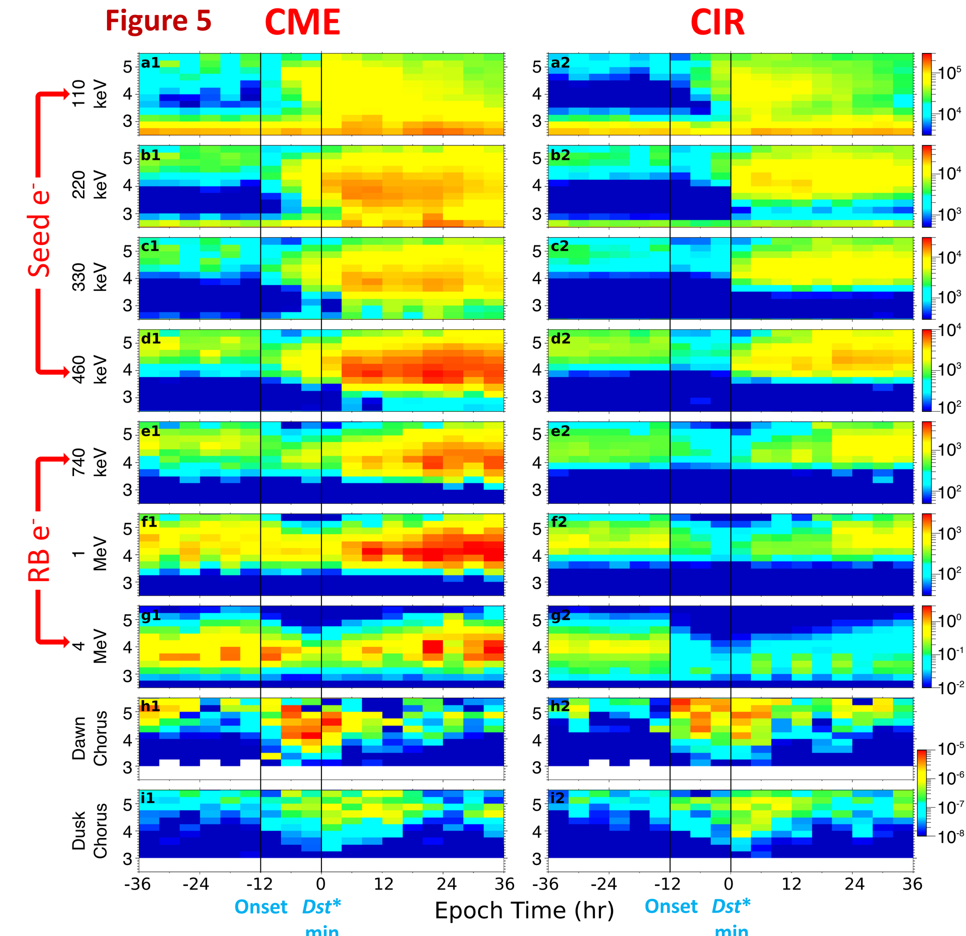

Figure 6

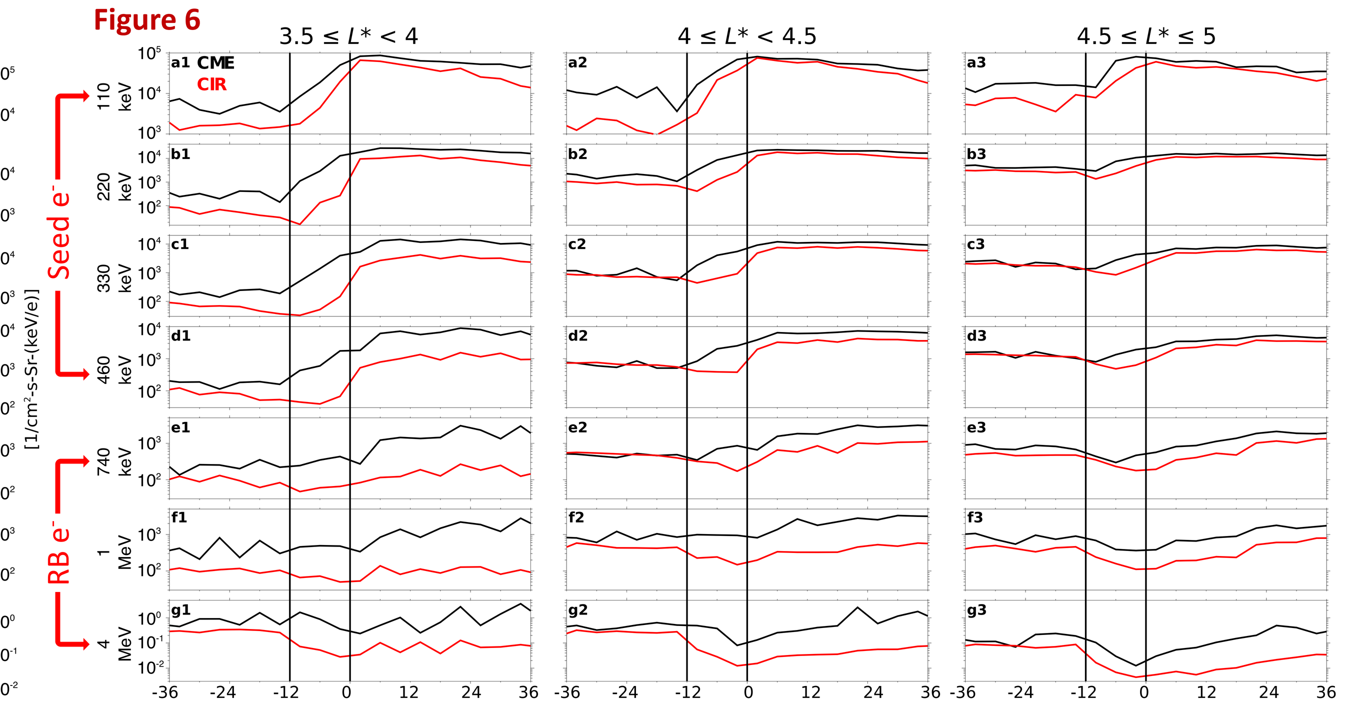

Figure 7

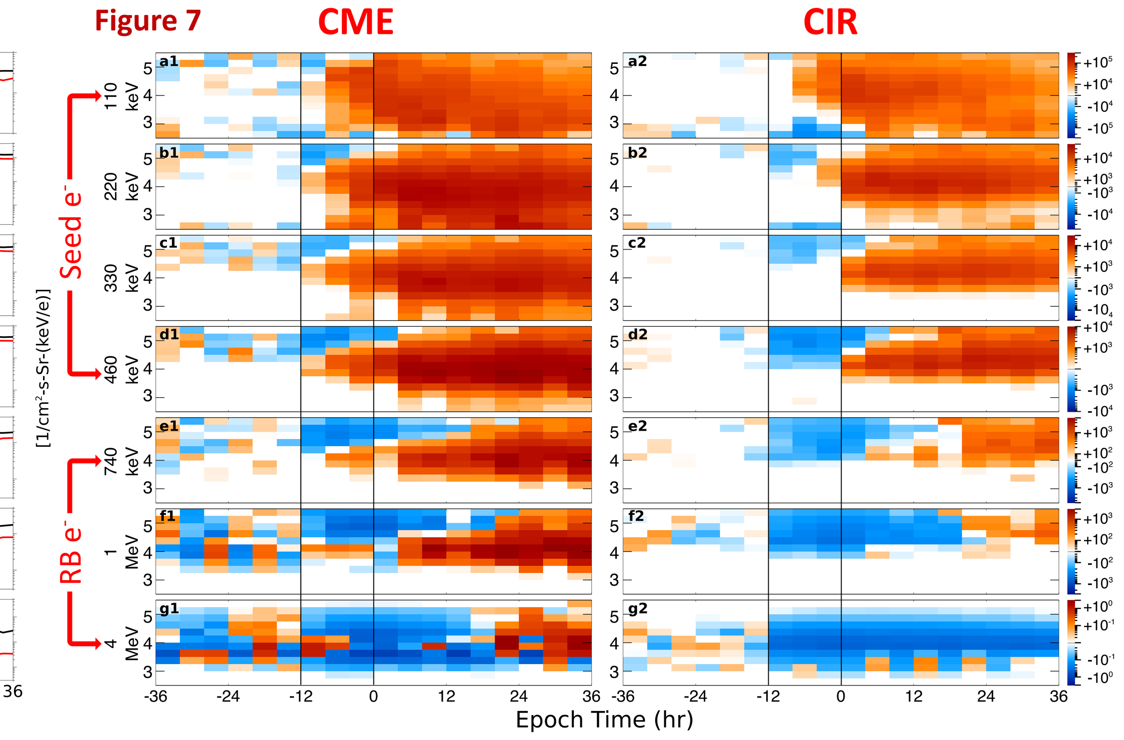

- **Stronger seed enhancement,** that **occurs earlier,** and **penetrates deeper** in **CME storms** over CIR storms.
- **Larger average radiation belt enhancement in CMEs.**
- **Earlier seed enhancement provides greater opportunity for local acceleration; more overlap of chorus with strong seed population.**

- **Greater substorm activity** and **convection** most **likely driving greater seed enhancement in CME** storms.
- **Stronger convection** and **more substorm** activity **gives higher energies more access** to **lower *L*** in the inner magnetosphere.

Phase Space Density Response

- Gradients of phase space density (PSD) can reveal aspects of the acceleration, transport, and loss of electron populations.
- Figure 8: average MagEIS PSD vs L^* for fixed μ and average chorus power.
- Figure 9: PSD in three different L^* ranges.
- Figure 10: Delta PSD - change in PSD from average prestorm levels vs L^*.

Figure 8

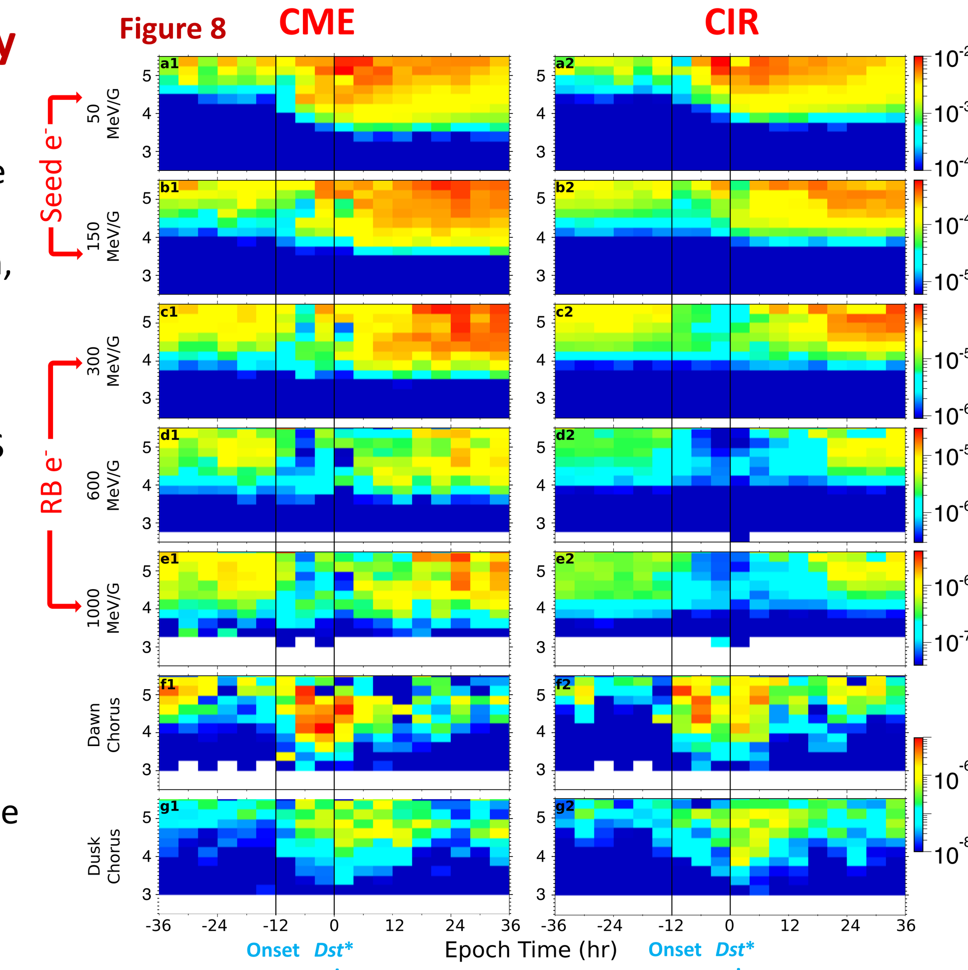

Figure 9

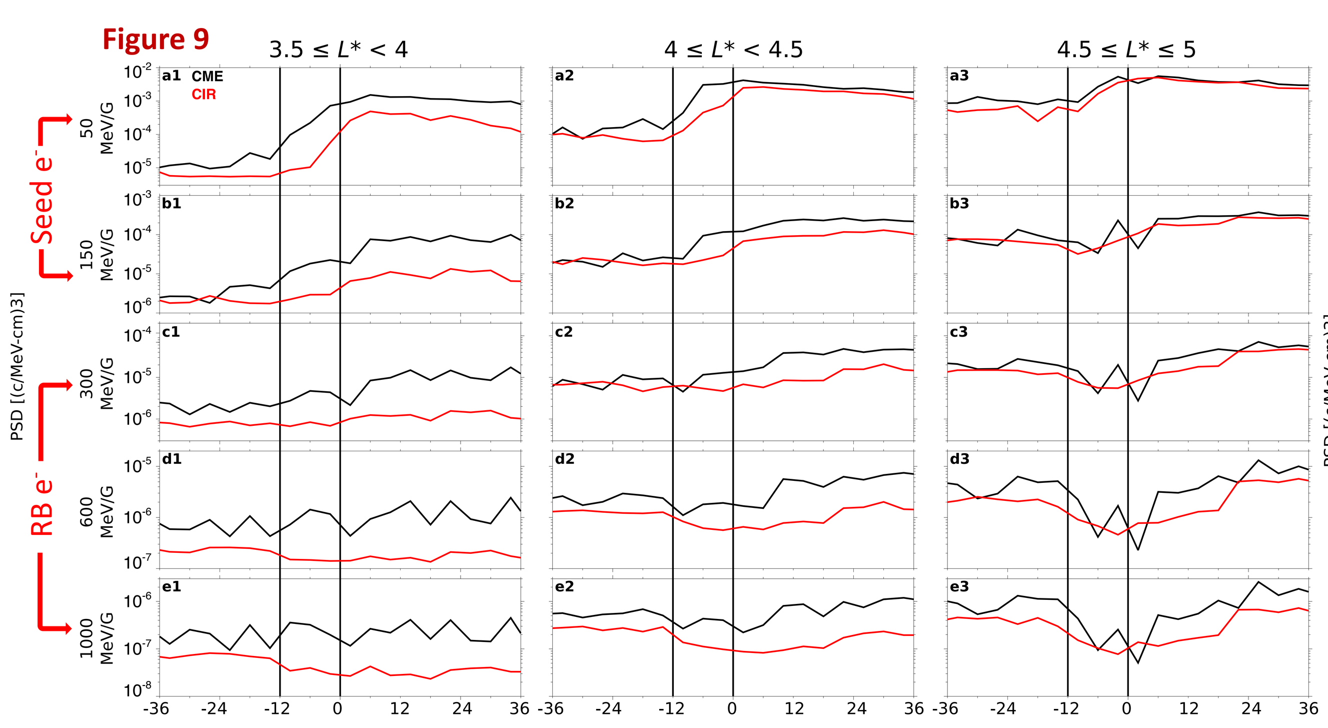

Figure 10

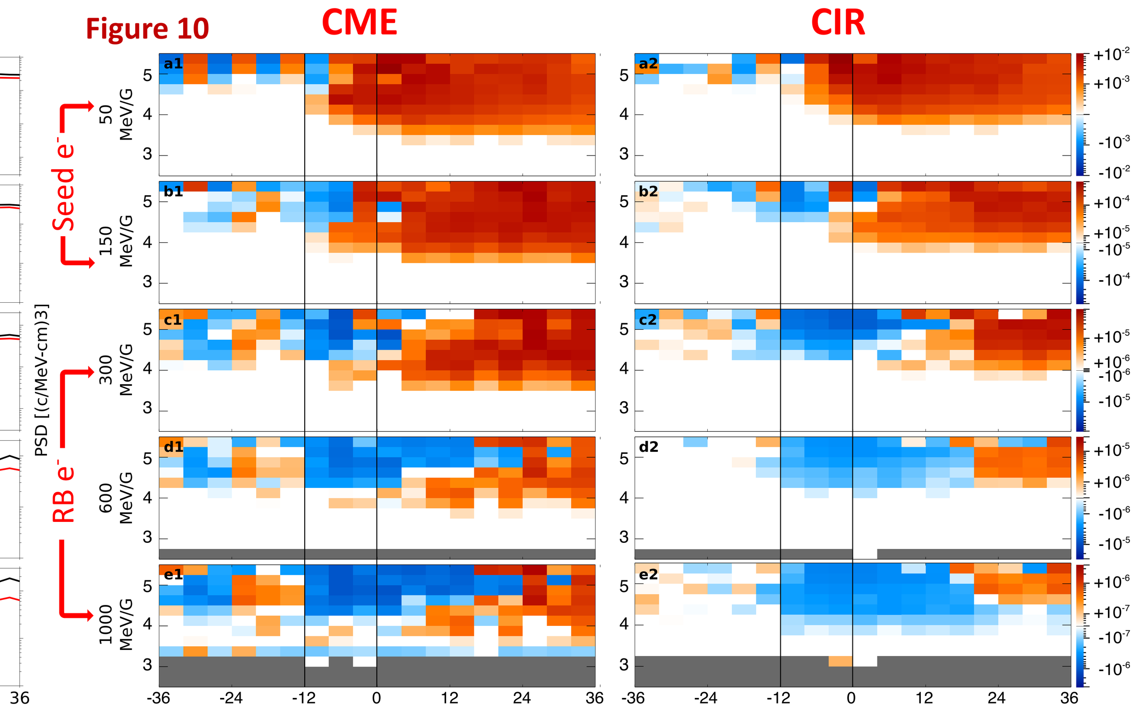

- **Stronger, earlier, and deeper seed PSD enhancement in CMEs.**
- **CME** 150 MeV/G **seed** population **reaches *Boyd et al.* [2015] threshold** of 1×10^{-4} (c/MeV-cm)^3 for acceleration **earlier and more often.**
- **CME Core population sees a greater net enhancement, which occurs 12-20 hours earlier, and occurs at lower L^*.**

- **Core enhancement in CMEs is during time with elevated levels of chorus activity.**
- **PSD profile of CME enhancement** shows a peak at inner L^* in recovery phase – **evidence of local acceleration.**